https://doi.org/10.5194/egusphere-2025-2787
Preprint. Discussion started: 4 July 2025

Atmospheric new particle formation in the eastern region of China: a mechanistic investigation at multiple sites

Jiaqi Jin[1], Runlong Cai[1,2,3,4], Yiliang Liu[1,a], Gan Yang[1], Yueyang Li[1], Chuang Li[1], Lei Yao[1,2,3,4], Jingkun Jiang[5,6], Xiuhui Zhang[7], Lin Wang[1,2,3,4,8]

[1]Department of Environmental Science and Engineering, Jiangwan Campus, Shanghai Key Laboratory of Atmospheric Particle Pollution and Prevention (LAP[3]), Fudan University, Shanghai 200438, China
[2]Shanghai Institute of Pollution Control and Ecological Security, Shanghai 200092, China
[3]IRDR International Center of Excellence on Risk Interconnectivity and Governance on Weather/Climate Extremes Impact and Public Health, Fudan University, Shanghai, China
[4]National Observations and Research Station for Wetland Ecosystems of the Yangtze Estuary, Shanghai, China
[5]State Key Joint Laboratory of Environmental Simulation and Pollution Control, School of Environment, Tsinghua University, Beijing, China.
[6]State Environmental Protection Key Laboratory of Sources and Control of Air Pollution Complex, Beijing, China.
[7]Key Laboratory of Cluster Science, Ministry of Education of China, School of Chemistry and Chemical Engineering, Beijing Institute of Technology, Beijing, China.
[8]Collaborative Innovation Center of Climate Change, Nanjing, 210023, China
[a]now at Chongqing Institute of Green and Intelligent Technology, Chinese Academy of Sciences, Chongqing 400714, China.

Correspondence to: Lin Wang (lin_wang@fudan.edu.cn)

Abstract. As a major source of cloud condensation nuclei, atmospheric new particle formation (NPF) events exert significant influences on the global climate. Among the various nucleation mechanisms that have been identified in diverse environments, sulfuric acid-amine nucleation is unique for its high efficiency to form stable clusters and drive intense nucleation. Despite the fact that this nucleation mechanism could explain observed NPF events at a number of megacity sites in China, its applicability to a larger regional scale remains unclear. Here, we analyzed characteristics of NPF events and influencing factors at three suburban sites in the eastern region of China based on measured and theoretically predicted particle formation rates and cluster concentrations. Results show that sulfuric acid-dimethylamine is a predominant nucleation mechanism at these sites, while atmospheric conditions including precursor concentrations and temperature causes the differences in NPF characteristics among different sites. This indicates the significance of the sulfuric acid-amine nucleation mechanism over a large spatial scale in the urban agglomerations in the eastern region of China. We also find that oxygenated organic molecules are likely involved in the formation of 1.7-nm new particles at these sites by contributing the initial growth of stable sulfuric acid clusters.

1 Introduction

New particle formation (NPF), an important atmospheric process involving the conversion of gaseous precursors into stable clusters via nucleation and subsequent growth, occurs frequently in diverse environments (Kerminen et al., 2018). It is a large source of the number concentration of atmospheric particles and significantly influences the budget of global cloud condensation nuclei (Gordon et al., 2017). Strong NPF events are frequently observed in polluted environments against the significant suppressing effect of background aerosols (Xiao et al., 2015; Hong et al., 2023). Among a number of nucleation mechanisms that were proposed recently (Kirkby et al., 2023), the clustering between sulfuric acid (SA) and dimethylamine (DMA) has been found to be a governing nucleation mechanism in polluted megacities for its high efficiency in forming clusters that are stable against evaporation (Yao et al., 2018; Cai et al., 2021). Recently, a relevant model study (Zhao et al., 2024) has indicated that SA-DMA is still the main nucleation mechanism in the atmospheric boundary layer of the polluted atmosphere on a larger regional scale, such as ~1M km^2 the population-dense area in the eastern region of China (Kulmala et

https://doi.org/10.5194/egusphere-2025-2787
Preprint. Discussion started: 4 July 2025

al., 2021). However, it remains to be explored through actual measurements.

Atmospheric NPF is often a regional-scale phenomenon spanning hundreds of kilometers (Kerminen et al., 2018). Simultaneous measurements at two or more stations have demonstrated the spatial heterogeneity of regional NPF characteristics such as the frequency of NPF events, the start time and duration of NPF events, and the formation and growth rates of new particles (Zhou et al., 2021; Dinoi et al., 2023; Shang et al., 2023). This heterogeneity of NPF is associated with the spatially heterogeneous distributions of diverse emission sources, complex urban morphology and meteorology, and the high selectivity and sensitivity of NPF to atmospheric conditions. The main causes of variations in the macroscopic characteristics of NPF remain to be verified. This urges a mechanistic exploration of NPF on a large regional scale, specifically, at multiple sites in the vast eastern part of China.

The influence of a number of factors needs to be accounted for when resolving nucleation mechanisms in the real atmosphere. Besides the concentrations of gaseous precursors and the scavenging loss of clusters and particles characterized by the condensation sink (CS), temperature also influences nucleation by altering the stability of clusters against evaporation (Olenius et al., 2017; Li et al., 2023). Global nucleation simulation using a three-dimensional model suggests that temperature was the second most important factor, following the concentration of precursors (Zhao et al., 2024). Laboratory studies have provided experimental evidence for the temperature dependence of sulfuric acid-amine nucleation at atmospheric-relevant amine concentrations (Xiao et al., 2021). Previous 1-year measurements in urban Beijing show that temperature governed the seasonal variations of NPF frequency and particle formation rate (Deng et al., 2020). It is also reasonable to expect a temperature dependence of NPF on a broad spatial scale, which remains to be addressed by observations.

The initial growth of freshly nucleated particles is important for NPF, as these smallest particles are most susceptible to scavenging losses. Previous studies proposed that SA and its clusters governs the initial growth in Chinese megacities, although the contributions from other condensable vapors, like OOMs, could not be excluded (Yao et al., 2018; Deng et al., 2020). OOMs were reported as the most important precursors for the subsequent growth of particles. Observational evidence from remote forests has demonstrated that the volatility distribution of OOMs can reasonably account for particle growth from 3 to 50 nm (Mohr et al., 2019). Similarly, in urban environments, a substantial proportion of particle growth occurring above 3 nm has been attributed to the condensation of OOMs (Qiao et al., 2021), indicating their ubiquitous role in both anthropogenically influenced and natural settings. Moreover, insights from controlled chamber studies also reinforced the potential role of OOMs in growth of newly-formed particle. In particular, some extremely low-volatility OOMs have been shown to promote directly to sub-3 nm initial growth of particles (Troestl et al., 2016; Stolzenburg et al., 2018). According to the results from laboratories, the contribution of OOMs to the initial growth of new particles is likely to be non-negligible in the real atmosphere, however, there has been insufficient ambient evidence for this suggestion.

To deepen the understanding of NPF in polluted atmospheres, we collected data measured at three suburban sites in the eastern part of China, including SA and DMA concentration ([SA] and [DMA]), OOMs concentrations ([OOMs]), cluster compositions, and particle size distribution (PSD) down to ~1 nm. The NPF mechanisms are analyzed after accounting for the effects of temperature and precursor concentrations on cluster concentration and particle formation rate. We also discuss the initial growth of new particles and explore the roles of OOMs in the formation of 1.7 nm particles.

2 Methods

2.1 Measurements

We conducted field campaigns at three suburban sites, namely Wangdu (WD), Dianshan Lake (DL) and Taihu Lake (TL). WD is located in Baoding, Hebei, with farmlands, forests and two highways nearby (Wang et al., 2020; Hu et al., 2022; Ren et al., 2022). DL is located in the southwest of Shanghai, surrounded by residential buildings, vegetation, a main traffic artery and a few industrial enterprises (Wu et al., 2023; Yang et al., 2023; Deng et al., 2025). Two campaigns were conducted at DL, one in winter (DLW) and the other in spring (DLS). TL is located in Wuxi, Jiangsu, surrounded by vegetation and a small number of settlements. The detailed information of these campaigns is given in Table 1.

A chemical ionization long time-of-flight mass spectrometer (CI-LToF-MS, Aerodyne Research, Inc.) was deployed to

https://doi.org/10.5194/egusphere-2025-2787
Preprint. Discussion started: 4 July 2025

measure gaseous SA, OOMs, and molecular clusters at these three sites (Lu et al., 2020). The mass spectrometer used nitrate and its clusters to ionize neutral molecules and clusters. A calibration coefficient derived from SA and a mass-to-charge-dependent transmission efficiency of the instrument were used to obtain [OOMs], assuming that they share the same kinetically controlled collision rate with reagent ions as that of SA.

A Vocus proton-transfer-reaction time-of-flight mass spectrometer (Vocus PTR-ToF-MS, Aerodyne Research Inc.) equipped with a focusing ion-molecular reactor (FIMR) was used at WD and DL, with modified instrument settings to measure DMA (Wang et al., 2020). A chemical ionization high-resolution time-of-flight mass spectrometer (CI-HToF-MS, Aerodyne Research Inc.) was used at TL with protonated ethanol or its hydrated clusters as reagent ions (Yao et al., 2016), to measure DMA. Since mass spectrometer cannot distinguish among isomers, C_2-amine was taken as DMA. NH_3 concentration ($[NH_3]$) was measured using the ion chromatography (IC) method of Chinese Standard (HJ 1076-2019) at WD and DL. There was no measurement for $[NH_3]$ at TL.

Particle size distribution (PSD) ranging from 1 to 3 nm was measured by an Airmodus A10 particle size magnifier (PSM). The PSD of 3-736 nm particles was measured by two scanning mobility particle sizers (SMPS TSI Inc, USA), namely a nano-SMPS and a long-SMPS (Yao et al., 2018). Temperature was monitored by an automatic weather station (Vaisala AWS310).

Furthermore, this study also involves ambient data previously reported at urban sites, namely Shanghai (SH, Yao et al., 2018) and Beijing (BJ, Cai et al., 2021; Qiao et al., 2021).

Table 1: The location, period and the usage of instrument at different sites.

Site	Location	Period	Instrument			
			SA & OOMs	DMA	NH_3	PSD
WD	38°39’ N, 115°11’ E	Dec. 2018-Jan. 2019	CI-LToF-MS	Vocus PTR-ToF-MS	CI	nano-SMPS+ long-SMPS+ PSM
DL	31°05’ N, 120°59’ E	Dec. 2022-Jan. 2023 & Apr. 2023-Jun. 2023				
TL	31°25’ N, 120°13’ E	Jul. 2023-Sep. 2023		HToF-CIMS	Not available	

2.2 Models

A cluster dynamics-multicomponent sectional model was applied to simulate SA-DMA nucleation process (Li et al., 2023). The model is composed of one cluster dynamics module and one sectional module. The detailed description of these two modules is given in the Supplement. SA tetramers were treated as nucleated particles for simulating particle formation rate at 1.4 nm diameter, $J_{1.4}$ (Larriba et al., 2011; Cai et al., 2021), and enter the sectional module as the smallest particles. Particle formation rate at 1.7 nm diameter, $J_{1.7}$, was simulated by incorporating the initial growth on the basis of $J_{1.4}$. However, in certain cases, this process could not be directly implemented in the model, because of data overflow. (Figure S1). Therefore, a survival probability approach was adopted as an alternative for the calculation (Cai et al., 2022a):

$$\frac{J_{\mathrm{p_1}}(t)}{J_{\mathrm{p_2}}(t)} = \exp \int_{d_{\mathrm{p2}}}^{d_{\mathrm{p1}}} -\frac{\mathrm{CoagS}(d_{\mathrm{p}})}{\mathrm{GR}(d_{\mathrm{p}})}\, \mathrm{d}d_{\mathrm{p}} \tag{1}$$

where d_{p1} is 1.7 nm, and d_{p2} is 1.4 nm, the corresponding particle size in calculating particle formation rates. The ratio $J_{1.4}/J_{1.7}$ is defined as the survival probability from 1.4 nm to 1.7 nm. GR is herein the simulated size-dependent growth rate, which is contributed by condensable vapors through the change of particle mass over time:

$$\frac{\mathrm{d}m_{\mathrm{p}}}{\mathrm{d}t} = \sum_i m_i \left(\alpha \beta_i N_i - \beta_i N_{i,\mathrm{sat}} \exp\left(\frac{4 v_i \sigma}{d_{\mathrm{p}} k_{\mathrm{B}} T} \right) f_i \right) \tag{2}$$

where m_{p} is the mass of particle; i represents each condensable species; m_i is the mass of molecules or clusters; α is the

https://doi.org/10.5194/egusphere-2025-2787
Preprint. Discussion started: 4 July 2025

accommodation coefficient, β_i is the collision constant between species i and the particle; $N_{i,sat}$ is the saturation concentration; v_i is the molecular volume, σ is the surface tension of the particle; k_B is the Boltzmann constant; and f_i is the molar fraction in the particle. In calculations, $(SA)_{1\text{-}4}(DMA)_{0\text{-}4}$ was treated as non-evaporative, meaning that they do not return to the gas phase after condensing on the particle.

2.3 Uncertainty analysis

The uncertainty of SA monomer concentration ($[SA_1]$) was estimated to be +100%/-50% (Cai et al., 2021). The uncertainty of [DMA] was +150%/-60% taking into account systematic and calibration uncertainties among campaigns (Freshour et al., 2014). The uncertainty of [OOMs] was expected to be greater than that of $[SA_1]$, because it was quantified by the calibration factor of SA. Li et al. (2023) reported that [OOMs] with a scaling factor of 1.35-4 could explain the measured new particle growth. Hence, the uncertainty of OOMs was estimated to be +200%/-66%. In terms of the volatility estimation of OOMs, the logarithm of saturation mass concentration ($\log C^*$) had an uncertainty of ±1 (Stolzenburg et al., 2018). The uncertainty of CS and measured -particle formation rate were ±10 % and +100%/-50%, respectively (Cai et al., 2021).

The uncertainties of simulated values, like the SA dimer concentration ($[SA_2]$) and the particle formation rate were obtained by inputting the extreme values of the uncertainty of measured data into the model. For example, the measured value of $[SA_1]$, [DMA] and CS were scaled by factors of 2, 2.5, and 1.1 (according to their uncertainty) were input to calculate the upper boundary of the uncertainty range of simulated $[SA_2]$ ($[SA_2]_{sim}$) and simulated $J_{1.4}$ ($J_{1.4,sim}$) and the lower boundary of simulated value was calculated in a similar way to the upper boundary, except that scale factors of 2, 2.5 and 1.1 were replaced by 0.5, 0.4 and 0.9, respectively.

2.4 Scaling processing

In order to better visualize the effects of $[SA_1]$ and temperature on SA dimer concentration and nucleation rate, we accounted the effects of CS and [DMA] by scaling the measured values to a same level based on simulation. Here, the scaling of measured $[SA_2]$ ($[SA_2]_{meas}$) is given as an example:

$$[SA_2]_{scaled} = [SA_2]_{meas} \cdot C(CS_{median}, [DMA]_{median}) \quad (3)$$

where $[SA_2]_{scaled}$ refers to the scaled $[SA_2]_{meas}$; $C(CS_{median}, [DMA]_{median})$ is the scaling coefficient for $[SA_2]_{meas}$, and was calculated by:

$$C(CS_{median}, [DMA]_{median}) = \frac{[SA_2]_{sim,median}}{[SA_2]_{sim}} \quad (4)$$

where $[SA_2]_{sim}$ is the simulated SA_2 concentration, which was calculated by inputting measured $[SA_1]$, [DMA], CS and temperature into the model; $[SA_2]_{sim,median}$ is calculated by inputting measured $[SA_1]$, measured temperature, the median [DMA] (2.3 pptv) and the median CS (0.017 s^{-1}) of all NPF events. $[SA_2]_{sim,median}$ can be regarded as the theoretical $[SA_2]_{meas}$ when measured [DMA] and CS reach the median values. [DMA] was not measured simultaneously with [SA] at SH. Considering high [DMA] (0.7-54.3 pptv) in other campaigns in urban Shanghai (Yao et al., 2016; Chang et al., 2021), [DMA] at SH was uniformly set at 5 pptv in scaling, at which $[SA_2]$ almost reached the nucleation limit under the atmospheric [SA] (Almeida et al., 2013). The scaling of the particle formation rate is given in detail in the Supplement.

3 Results and discussion

3.1 SA-DMA nucleation for all the campaigns

Figure 1 shows the measured particle formation rates at 1.7 nm diameter ($J_{1.7,meas}$) as a function of $[SA_1]$ and compares them with measured results of other campaigns. Our data, except for that at TL, is accord with SA-DMA-NH_3(-OOMs) nucleation at 293 K of Cosmics Leaving Outdoor Droplets (CLOUD) experiments. Data at TL follows the simulated lines for SA-DMA nucleation at 303 K. Furthermore, our observed results are also close to those at SH and BJ, where SA and DMA have been proved to play key roles in nucleation (Yao et al., 2018; Cai et al., 2021), meaning that nucleation mechanisms among them

https://doi.org/10.5194/egusphere-2025-2787
Preprint. Discussion started: 4 July 2025

are very likely to be consistent. Our campaigns had higher CS and lower [DMA] than the experimental conditions of CLOUD (Table 2), both of which are unfavorable for $J_{1.7}$. This provides an explanation for the generally lower $J_{1.7,meas}$ observed in our measurements compared to those from CLOUD under varying temperature conditions. Particle formation rates under SA-DMA nucleation remain almost unchanged after adding certain [NH_3] and [OOMs] in CLOUD (Kürten et al., 2018; Xiao et al., 2021), and our observations show a close level of [NH_3] and relatively low [OOMs] compared with CLOUD experiments (Table 2). It is difficult to determine whether NH_3 and OOMs participate in nucleation based on particle formation rate solely. Therefore, the dominate NPF mechanism in our campaigns was identified as SA-DMA.

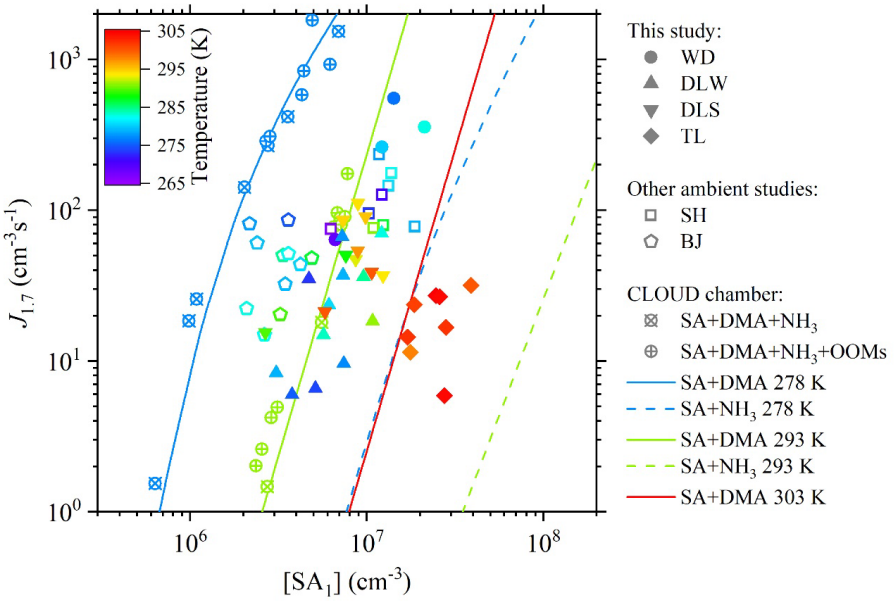

Figure 1: $J_{1.7,meas}$ as a function of [SA_1] with the comparison of ambient data and CLOUD. Rainbow filled symbols represent measured data in this study, indicating one NPF events with the time resolution of 30 min, which were selected when $J_{1.7,meas}$ reaches maximum. Rainbow open symbols represent data from published studies (Yao et al., 2018; Cai et al., 2021). Symbols with crosses indicate CLOUD data in the temperature of 278 K and 293 K, respectively. Lines represent the fitting result of CLOUD (Xiao et al., 2021), except for the SA-DMA fitting at 303 K that is derived from the CLOUD fitting line of SA+DMA 293 K by the cluster dynamics-multicomponent sectional model.

https://doi.org/10.5194/egusphere-2025-2787
Preprint. Discussion started: 4 July 2025

Table 2: Comparison of NPF characteristics in different campaigns.

Dada source		Temperature (K)	CS (s^{-1})	[DMA] (pptv)	[OOMs] (cm^{-3})	[NH_3] (ppbv)
This study	median	290	0.017	2.3	1.8×10^8	2.1
	range	268-307	0.008-0.060	0.6-18.3	2.0×10^7-9.7×10^8	0.4-7
CLOUD (Xiao et al., 2021)		278, 293	0.002-0.008	4	up to 8.8×10^9	1-2.5
Shanghai (Yao et al., 2018)		267-291	0.017-0.039	-	2.3×10^7-2.1×10^8	-
Beijing (Cai et al., 2021; Qiao et al., 2021)		275-289	0.005-0.021	0.7-3.5	1.2×10^7-6.4×10^7	0.3-2.3

The measured cluster composition provides observational evidence for the involvement of DMA in the formation of SA clusters, while other base molecules were not detected (Figure 2). A number of neutral clusters, including SA and SA-DMA clusters, along with S-O based ions, were observed at WD, DL and TL. These clusters are described as SA monomer (SA_1), dimer (SA_2), trimers ($SA_3DMA_{0\text{-}2}$) and tetramers ($SA_4DMA_{1\text{-}2}$), contributing to NPF. The absence of DMA in SA monomer and dimer clusters are caused by their loss in the mass spectrometer (Cai et al., 2022b). Similar patterns of SA-DMA clusters were also measured at SH (Yao et al., 2018) and BJ (Yin et al., 2021). Other clusters related to nucleation, like SA-OOMs and SA-NH_3, were not observed, but the possibility that NH_3 and OOMs participate in nucleation cannot be ruled out, as they are generally present in the detection of ion clusters, rather than neutral clusters (Yin et al., 2021; Cai et al., 2024). The accordant comparison of simulated and measured [SA_2], and the temperature dependence of nucleation also give further support for that SA-DMA nucleation, which is described specifically in the Sect. 3.2.

https://doi.org/10.5194/egusphere-2025-2787
Preprint. Discussion started: 4 July 2025

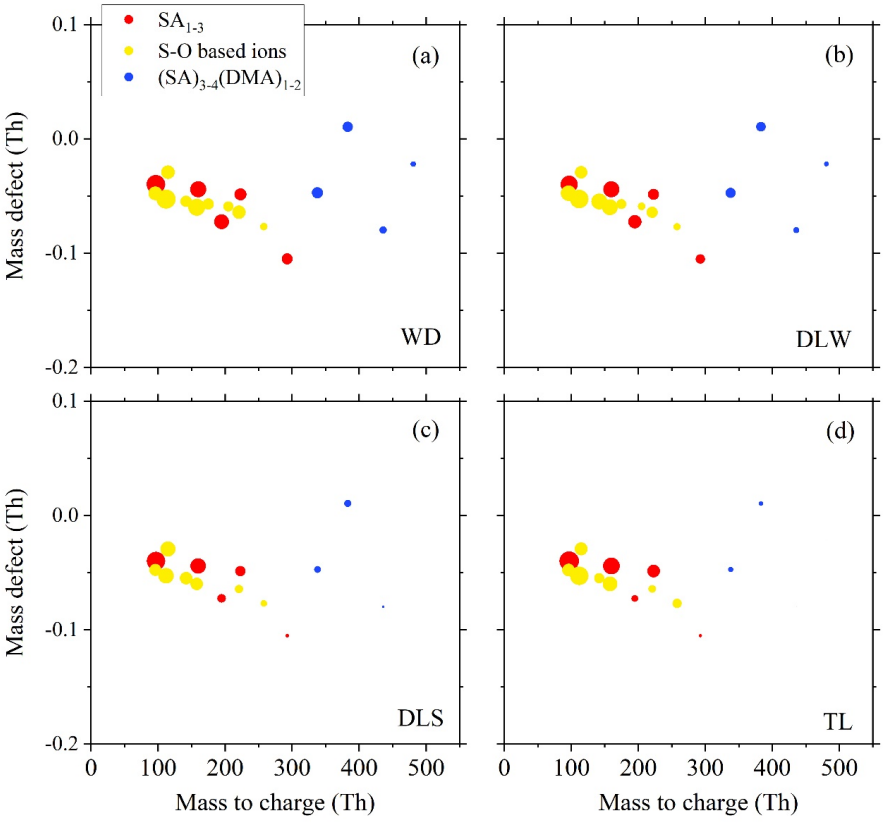

Figure 2: The mass defect of SA molecules, its clusters, and S-O based ions during four NPF events on (a) January 20th, 2019 in WD (temperature = 275 K; [SA_1] = 1.4×10^7 cm^{-3}; CS =0.055 s^{-1}; [DMA] = 3.4 pptv); (b) January 27th, 2023 in DLW (temperature = 277 K; [SA_1] = 7.3×10^6 cm^{-3}; CS =0.012 s^{-1}; [DMA] = 1.5 pptv); (c) May 2nd, 2023 in DLS (temperature = 295 K; [SA_1] = 9.5×10^6 cm^{-3}; CS =0.014 s^{-1}; [DMA] = 2.9 pptv); (d) August 7th, 2023 in TL (temperature = 304 K; [SA_1] = 2.6×10^7 cm^{-3}; CS =0.023 s^{-1}; [DMA] = 1.8 pptv). The symbol size is proportional to the logarithm of the normalized signal intensity.

We further analyze the factors determining the occurrence of NPF events in different campaigns by contrasting NPF and non-NPF events (Figure 3). [SA_1] is key to determining the occurrence of NPF at DL and TL, with the median values of [SA_1] being 1-2 times higher in NPF periods compared to those in non-NPF periods (Figure 3a). Similarly, CS during NPF periods is generally lower than that during non-NPF days in all campaigns, except DLS, further confirming that high preexisting aerosols are able to suppress the occurrence of NPF (Figure 3b). It contrasts with patterns in Po Valley, where CS remained at similar levels regardless of whether NPF occurs (Cai et al., 2024). Other potential precursors related to nucleation, including DMA, OOMs and NH_3 seem to have no notable influence on the occurrence of NPF in all campaigns, since their concentrations during NPF periods were not obviously higher than those during non-NPF periods (Figure S2). Similarly, temperature does not appear to be a decisive factor determining the occurrence of NPF (Figure 3c), but it exerts a considerable influence on the intensity of NPF among campaigns, as elaborated in the next paragraph.

The comparison among different campaigns indicates that [SA_1] and temperature played key roles in determining the intensity of NPF indicated by $J_{1.7,meas}$ (Figure 3d). Although [SA_1] at TL is the highest at all sites, high temperature (298-306 K) at TL resulted in lower median values of $[SA_2]_{meas}$ and $J_{1.7,meas}$ than those at other sites. In contrast, WD has the lowest temperature (281-268 K) and relatively high [SA_1] (7×10^6-1.8×10^7 cm^{-3}) in all campaigns. Even under strong coagulation scavenging effect (median CS = ~0.05 s^{-1}), $J_{1.7,meas}$ at WD are the highest (~310 $cm^{-3}s^{-1}$). The effect of temperature on NPF was also considerable in the analysis of other observations in Beijing in different seasons (Deng et al., 2020).

https://doi.org/10.5194/egusphere-2025-2787
Preprint. Discussion started: 4 July 2025

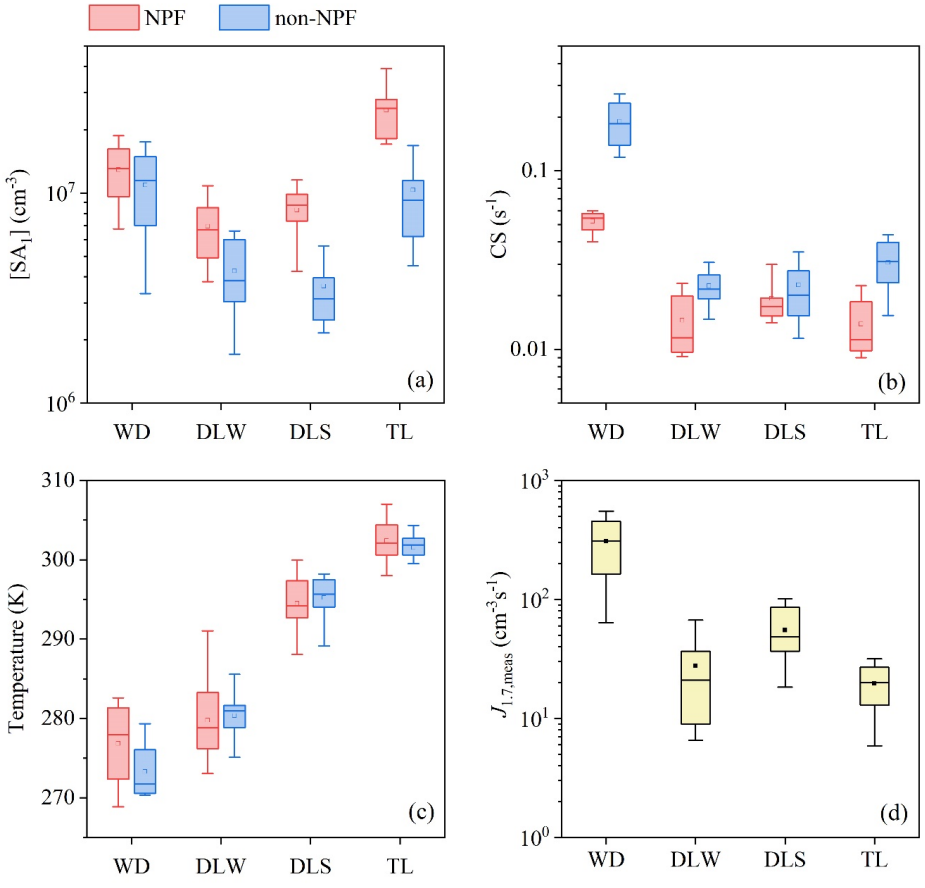

Figure 3: Parameters related to NPF. (a) [SA_1], (b) CS, (c) temperature during NPF periods and non-NPF periods, and (d) $J_{1.7,meas}$ during NPF periods. The NPF period is defined as the period with the maximum value of $J_{1.7}$ in each NPF event, and the non-NPF period is defined as the median range of all NPF periods (9:00-11:00) in non-NPF days. In order to eliminate the influence of precipitation, only sunny and cloudy days are selected for non-NPF. The transverse lines and square markers inside the boxes indicate mean values and median values, respectively. The bottom and top edges of the box indicate the 25th and 75th percentiles, respectively. The bottom and top edges of the whisker lines outside of the boxes indicate the 10th and 90th percentiles, respectively.

3.2 Temperature dependence of nucleation

To focus on the influence of [SA_1] and temperature on nucleation, and minimize the influence of other influencing factors, namely [DMA] and CS, on nucleation, we scaled the measured data to the median [DMA] and CS (see Methods). Figure 4 shows the comparison between $[SA_2]_{sim}$ and $[SA_2]_{meas}$, in which $[SA_2]_{meas}$ is in an agreement with the corresponding $[SA_2]_{sim}$, considering the uncertainty range in its measurement. To be specific, the $[SA_2]_{meas}$ is slightly lower than the simulated value, and this systematic discrepancy is likely due to measurement errors. It is possible that not all SA_2 is fully detected, as some of them may have dissociated within the mass spectrometer (Zapadinsky et al., 2019). The comparison of measured and simulated $J_{1.4}$ is shown in Figure S3, and the simulation results are acceptable through uncertainty analysis. In addition to supporting our argument that SA-DMA clustering can explain the formation of stable SA dimers, this agreement between $[SA_2]_{sim}$ and $[SA_2]_{meas}$, also provides supports for the feasibility to use simulation for of data scaling.

https://doi.org/10.5194/egusphere-2025-2787
Preprint. Discussion started: 4 July 2025

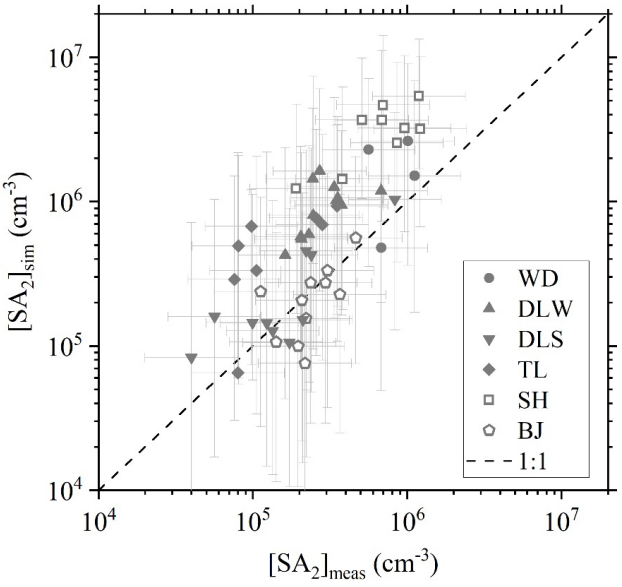

Figure 4: The comparison between $[SA_2]_{meas}$ and $[SA_2]_{sim}$. Horizontal and vertical error bars connected with each symbol indicate the uncertainties of x-axis and y-axis, respectively.

After accounting for the influence of CS and [DMA], we find that $[SA_2]_{scaled}$ show a significant decreasing trend with an increasing temperature, which is in a decent consistency with the simulated results (Figure 5). For every 20 K increase in temperature, the $[SA_2]_{scaled}$ descends by approximately one order of magnitude. This trend underscores the dominant influence of temperature in governing the stability and abundance of clusters in nucleation pathways. The temperature dependence of the ratio of $[SA_2]$ to $[SA_1]$ is also corroborated by previous studies focusing on SA-DMA nucleation. (Almeida et al., 2013; Yao et al., 2018). On the molecular level, DMA acts as a kind of stable nucleating agent. Most of SA firstly converts into SA_1DMA_1 and then forms SA dimer subsequently (Cai et al., 2022b). SA_1DMA_1 has relatively low thermal stability (Ortega et al., 2012; Myllys et al., 2019), which explains the temperature effect on $[SA_2]$ mechanistically. The effect of temperature can also be reflected in larger clusters, like SA trimer and tetramer (Figure 2). Even though the high-temperature (303 K) NPF period at TL had the higher $[SA_1]$ (~2.6×10^7 cm^{-3}), the abundance and variety of measured cluster were lower than those on low-temperatures (275 K and 277 K) at WD and DLW. In addition to temperature, the effect of [DMA] on $[SA_2]$ was also described in Figure S4. The rise in [DMA] considerably promotes the generation of SA_2, the promotion efficiency is gradually not obvious meanwhile, because [DMA] is close to nucleation saturation (Almeida et al., 2013).

https://doi.org/10.5194/egusphere-2025-2787
Preprint. Discussion started: 4 July 2025

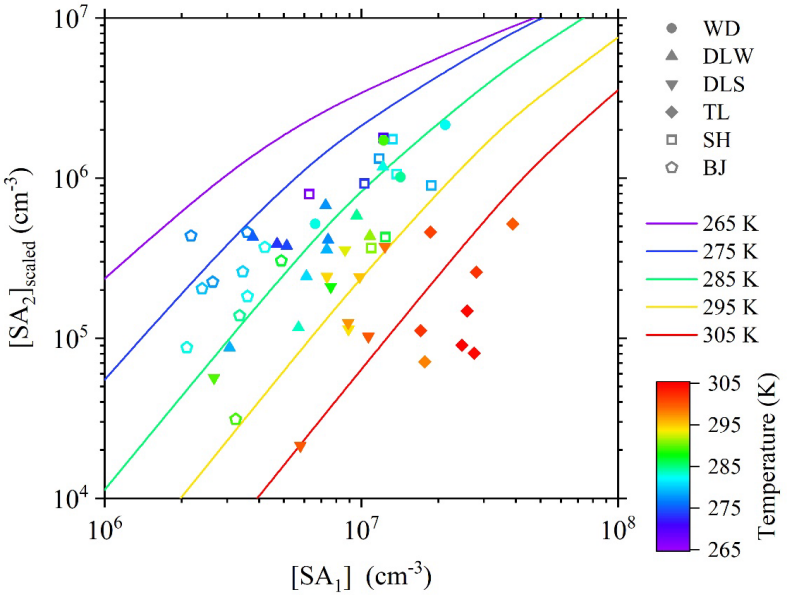

Figure 5: $[SA_2]_{scaled}$ as a function of $[SA_1]$ under a temperature gradient. Each symbol indicates one NPF event with a time resolution of 30 min, which was selected when $J_{1.7,meas}$ reaches maximum. [DMA] and CS for the simulated lines calculated by the discrete-sectional model are their median values in all NPF events, i.e., 0.017 s^{-1} and 2.3 pptv, respectively. To visualize the effect of temperature, the color of the simulated lines corresponds to the color bar.

The significant effect of temperature on cluster stability further causes large differences in $J_{1.4}$ (Figure 6). Specifically, the values of scaled $J_{1.4}$ ($J_{1.4,scaled}$) span approximately 3 orders of magnitude for the same $[SA_1]$ over a temperature range of about 30 K. This highlights the critical role of temperature in modulating nucleation, suggesting that temperature fluctuations can lead to substantial variability in NPF without the change in the major nucleation precursors. In other words, SA and DMA can still explain the wide range of $J_{1.4,scaled}$ at these sites. In terms of trends, $J_{1.4,scaled}$ exhibits a negative correlation with temperature, which is consistent with published atmospheric investigations (Yu et al., 2016; Deng et al., 2020). Similar to $[SA_2]$, the evaporation rate of SA_1DMA_1 is a key factor influencing the temperature dependence of particle formation rate (Deng et al., 2020; Cai et al., 2022b). It is evident that the temperature dependence of $J_{1.4}$ was not as pronounced as that of SA_2, particularly data points at DL, which are clustered together with the temperature range of ~20 K. Some of them also correspond worse to the simulated results, compared with data points in other campaigns. The temperature dependence of $J_{1.4}$ at DL was obvious in the inter-comparison of each campaign (Figure S5), when all campaigns collectively analyzed, the presentation of temperature dependence is subject to systematic uncertainties across different campaigns.

https://doi.org/10.5194/egusphere-2025-2787
Preprint. Discussion started: 4 July 2025

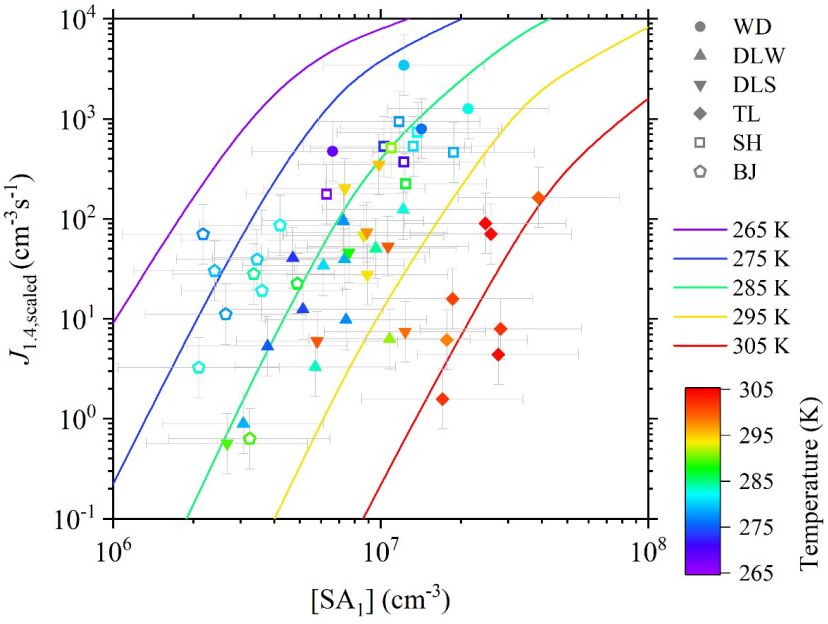

Figure 6: $J_{1.4,scaled}$ as a function of [SA$_1$] under the temperature gradient. Each symbol indicates one NPF events with a time resolution of 30 min, which were selected when $J_{1.7,meas}$ reaches maximum. [DMA] and CS for the simulated lines by the discrete-sectional model are their median values in all NPF events, i.e., 0.017 s^{-1} and 2.3 pptv, respectively. Horizontal and vertical error bars connected with each symbol indicate the uncertainties of x-axis and y-axis, respectively. To visualize the effect of temperature, the color of the simulated lines corresponds to the color bar.

3.3 Initial growth of nucleated particles

The discussions above have shown that SA-DMA nucleation could explain predominant nucleation mechanism at five sites. Here, we investigate the contribution of particle initial growth to $J_{1.7}$. Figure 7a presents the comparison of simulated growth rate of 1.4-1.7 nm particles ($GR_{1.4\text{-}1.7}$) with two groups of condensable vapors at BJ and DLS. When only the contribution of sulfuric acid is considered, the $GR_{1.4\text{-}1.7}$ values at the two sites range approximately from 0.3 to 3.4 nm/h. If $GR_{1.4\text{-}1.7}$ could be roughly approximated to growth rate of under 3 nm particles, these values of simulated $GR_{1.4\text{-}1.7}$ are in accordance with the measured range (0.5-14.3 nm/h) in previous reports from the eastern region of China (Xiao et al., 2015; Dai et al., 2017; Yao et al., 2018; Hong et al., 2023). The simulated $GR_{1.4\text{-}1.7}$ is enhanced when OOMs are also considered as condensable vapors on the basis of the contribution of SA and its clusters. The same comparison in other four campaigns is shown in Figure S6a.The volatility distribution of observed OOMs for simulating is shown in Figure S7. Here, it is assumed that only SA, its clusters and OOMs contribute to $GR_{1.4\text{-}1.7}$, because they can largely explain the growth of particles in urban areas (Qiao et al., 2021).

The simulation of $J_{1.7}$ is improved by considering the contribution of OOMs to the initial growth of new particles. The comparison between $J_{1.7,meas}$ and the simulated $J_{1.7}$ ($J_{1.7,sim}$) at BJ and DLS is shown in Figure 7b. When merely considering the contribution of SA and its clusters to GR, there is a significant deviation between the values of $J_{1.7,meas}$ and $J_{1.7,sim}$ generally, and some of them even deviated by more than 3 orders of magnitude. Compared to the simulation of $J_{1.4}$ (Figure S2), the values of $J_{1.7,sim}$ at DLS and BJ also reveal an evident decline. After incorporating the contribution of OOMs to $GR_{1.4\text{-}1.7}$, the values of $J_{1.7,sim}$ are greatly elevated. The corresponding results of improvement are poor at WD, DLW, TL and SH, and the contribution of SA and its clusters seems sufficient to explain $GR_{1.4\text{-}1.7}$ in these campaigns (Figure S6b). In fact, OOMs may also be involved in clustering, especially at DL and TL with high concentrations of ultralow volatile organic compounds (Figure S7), which are capable of nucleating (Simon et al., 2020). Nevertheless, regardless of their contribution to nucleation, their effects on condensation were also considerable to $J_{1.7}$, which also demonstrates strong temperature dependence like $J_{1.4}$ (Figure

https://doi.org/10.5194/egusphere-2025-2787
Preprint. Discussion started: 4 July 2025

S8).

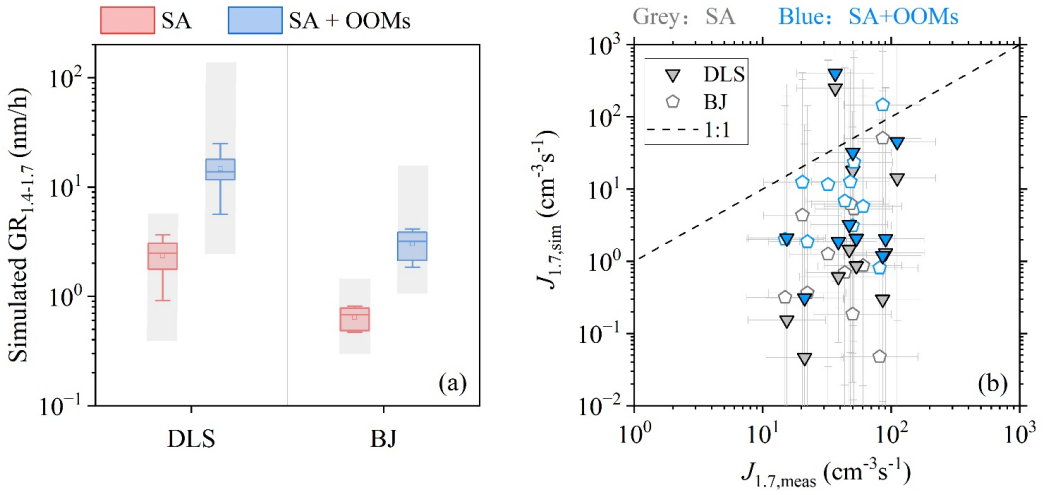

Figure 7: The simulation of $GR_{1.4\text{-}1.7}$ and $J_{1.7}$. (a) The comparison of simulated $GR_{1.4\text{-}1.7}$ contributed by SA and its clusters (i.e. SA in the legend), as well as SA and its clusters plus OOMs in campaigns. The transverse lines and square markers inside the boxes indicate mean values and median values, respectively. The bottom and top edges of the box indicate the 25th and 75th percentiles, respectively. The bottom and top edges of the whisker lines outside of the boxes indicate the 10th and 90th percentiles, respectively. The shade boxes indicate the ranges of uncertainties. (b)The comparison between $J_{1.7,meas}$ and $J_{1.7,sim}$. Horizontal and vertical error bars connected with each symbol indicate the uncertainties of x-axis and y-axis, respectively.

4 Conclusions

We analyze the governing mechanism SA-DMA in the eastern region of China using observation data at three sites, including the concentrations of key chemical species, meteorological parameters and PSD. Both the nucleating clusters, exemplified by SA_2, and the nucleation rates, represented by $J_{1.4}$, can be attributed to the collisions between SA and DMA to a large extent. However, SA and its clusters are insufficient, at least at DSL and BJ, to explain the initial growth of freshly nucleated particles, while OOMs make great contribution to this process. Given the considerable spatial separation among the five sites, it is thus inferred that within this geographical scope, SA and DMA are capable of describing atmospheric nucleation up to 1.4 nm, whereas OOMs are involved in $GR_{1.4\text{-}1.7}$, thereby improving the simulation performance of $J_{1.7}$, which is derived from model-observation comparisons, and direct experimental evidence remains to be substantiated. Besides, the effect of temperature on SA-DMA nucleation was illustrated quantitatively through scaling, and the differences in nucleation intensity among campaigns could also be demonstrated by variations in temperature under the same mechanism. With the notable reduction in $[SO_2]$ and [amines] in recent years (Liu et al., 2023; Du et al., 2025), and the strong dependence of $[SO_2]$ on $[SA_1]$ production (Lu et al., 2019), the applicability of SA-DMA mechanism to atmospheric nucleation over a wide spatial scale in the eastern region of China, as well as other densely populated and polluted regions may continually evolve, which warrants further investigation in the future.

References

Almeida, J., Schobesberger, S., Kuerten, A., Ortega, I. K., Kupiainen-Maatta, O., Praplan, A. P., Adamov, A., Amorim, A., Bianchi, F., Breitenlechner, M., David, A., Dommen, J., Donahue, N. M., Downard, A., Dunne, E., Duplissy, J., Ehrhart, S., Flagan, R. C., Franchin, A., Guida, R., Hakala, J., Hansel, A., Heinritzi, M., Henschel, H., Jokinen, T., Junninen, H., Kajos,

https://doi.org/10.5194/egusphere-2025-2787
Preprint. Discussion started: 4 July 2025

M., Kangasluoma, J., Keskinen, H., Kupc, A., Kurten, T., Kvashin, A. N., Laaksonen, A., Lehtipalo, K., Leiminger, M., Leppa, J., Loukonen, V., Makhmutov, V., Mathot, S., McGrath, M. J., Nieminen, T., Olenius, T., Onnela, A., Petaja, T., Riccobono, F., Riipinen, I., Rissanen, M., Rondo, L., Ruuskanen, T., Santos, F. D., Sarnela, N., Schallhart, S., Schnitzhofer, R., Seinfeld, J. H., Simon, M., Sipila, M., Stozhkov, Y., Stratmann, F., Tome, A., Troestl, J., Tsagkogeorgas, G., Vaattovaara, P., Viisanen, Y., Virtanen, A., Vrtala, A., Wagner, P. E., Weingartner, E., Wex, H., Williamson, C., Wimmer, D., Ye, P., Yli-Juuti, T., Carslaw, K. S., Kulmala, M., Curtius, J., Baltensperger, U., Worsnop, D. R., Vehkamaki, H., and Kirkby, J.: Molecular understanding of sulphuric acid-amine particle nucleation in the atmosphere, Nature, 502, 359–363, https://doi.org/10.1038/nature12663, 2013.

Cai, J., Sulo, J., Gu, Y., Holm, S., Cai, R., Thomas, S., Neuberger, A., Mattsson, F., Paglione, M., Decesari, S., Rinaldi, M., Yin, R., Aliaga, D., Huang, W., Li, Y., Gramlich, Y., Ciarelli, G., Quéléver, L., Sarnela, N., Lehtipalo, K., Zannoni, N., Wu, C., Nie, W., Kangasluoma, J., Mohr, C., Kulmala, M., Zha, Q., Stolzenburg, D., and Bianchi, F.: Elucidating the mechanisms of atmospheric new particle formation in the highly polluted Po Valley, Italy, Atmos. Chem. Phys., 24, 2423–2441, https://doi.org/10.5194/acp-24-2423-2024, 2024.

Cai, R., Yan, C., Yang, D., Yin, R., Lu, Y., Deng, C., Fu, Y., Ruan, J., Li, X., Kontkanen, J., Zhang, Q., Kangasluoma, J., Ma, Y., Hao, J., Worsnop, D. R., Bianchi, F., Paasonen, P., Kerminen, V.-M., Liu, Y., Wang, L., Zheng, J., Kulmala, M., and Jiang, J.: Sulfuric acid-amine nucleation in urban Beijing, Atmos. Chem. Phys., 21, 2457–2468, https://doi.org/10.5194/acp-21-2457-2021, 2021.

Cai, R., Deng, C., Stolzenburg, D., Li, C., Guo, J., Kerminen, V.-M., Jiang, J., Kulmala, M., and Kangasluoma, J.: Survival probability of new atmospheric particles: closure between theory and measurements from 1.4 to 100 nm, Atmos. Chem. Phys., 22, 14571–14587, https://doi.org/10.5194/acp-22-14571-2022, 2022a.

Cai, R., Yin, R., Yan, C., Yang, D., Deng, C., Dada, L., Kangasluoma, J., Kontkanen, J., Halonen, R., Ma, Y., Zhang, X., Paasonen, P., Petaja, T., Kerminen, V.-M., Liu, Y., Bianchi, F., Zheng, J., Wang, L., Hao, J., Smith, J. N., Donahue, N. M., Kulmala, M., Worsnop, D. R., and Jiang, J.: The missing base molecules in atmospheric acid-base nucleation, Natl. Sci. Rev., 9, nwac137, https://doi.org/10.1093/nsr/nwac137, 2022b.

Chang, Y., Gao, Y., Lu, Y., Qiao, L., Kuang, Y., Cheng, K., Wu, Y., Lou, S., Jing, S., Wang, H., and Huang, C.: Discovery of a potent source of gaseous amines in urban China, Environ. Sci. Technol. Lett., 8, 725–731, https://doi.org/10.1021/acs.estlett.1c00229, 2021.

Dai, L., Wang, H., Zhou, L., An, J., Tang, L., Lu, C., Yan, W., Liu, R., Kong, S., Chen, M., Lee, S., and Yu, H.: Regional and local new particle formation events observed in the Yangtze River Delta region, China, J. Geophys. Res.-Atmos., 122, 2389–2402, https://doi.org/10.1002/2016JD026030, 2017.

Deng, C., Fu, Y., Dada, L., Yan, C., Cai, R., Yang, D., Zhou, Y., Yin, R., Lu, Y., Li, X., Qiao, X., Fan, X., Nie, W., Kontkanen, J., Kangasluoma, J., Chu, B., Ding, A., Kerminen, V.-M., Paasonen, P., Worsnop, D. R., Bianchi, F., Liu, Y., Zheng, J., Wang, L., Kulmala, M., and Jiang, J.: Seasonal characteristics of new particle formation and growth in urban Beijing, Environ. Sci. Technol., 54, 8547–8557, https://doi.org/10.1021/acs.est.0c00808, 2020.

Deng, K., Huo, J., Wang, Y., Wang, L., Yin, S., Li, C., Li, Y., Yang, G., Yao, L., Fu, Q., and Wang, L.: Characteristics of atmospheric reduced-sulfur compounds at a suburban site of Shanghai, J. Environ. Sci., 156, 671–683, https://doi.org/10.1016/j.jes.2024.06.030, 2025.

Dinoi, A., Gulli, D., Weinhold, K., Ammoscato, I., Calidonna, C. R., Wiedensohler, A., and Contini, D.: Characterization of ultrafine particles and the occurrence of new particleformation events in an urban and coastal site of the Mediterranean area, Atmos. Chem. Phys., 23, 2167–2181, https://doi.org/10.5194/acp-23-2167-2023, 2023.

Du, W., Jiang, S., Fu, N., Song, J., Lin, X., Mao, K., Shi, J., Chen, Y., Liu, J., and Tao, S.: Ammonia and amines emissions from residential biomass combustion in China from 2014 to 2030, J. Hazard. Mater., 488, 137476, https://doi.org/10.1016/j.jhazmat.2025.137476, 2025.

Freshour, N. A., Carlson, K. K., Melka, Y. A., Hinz, S., Panta, B., and Hanson, D. R.: Amine permeation sources characterized with acid neutralization and sensitivities of an amine mass spectrometer, Atmos. Meas. Tech., 7, 3611–3621, https://doi.org/10.5194/amt-7-3611-2014, 2014.

Gordon, H., Kirkby, J., Baltensperger, U., Bianchi, F., Breitenlechner, M., Curtius, J., Dias, A., Dommen, J., Donahue, N. M.,

https://doi.org/10.5194/egusphere-2025-2787
Preprint. Discussion started: 4 July 2025

Dunne, E. M., Duplissy, J., Ehrhart, S., Flagan, R. C., Frege, C., Fuchs, C., Hansel, A., Hoyle, C. R., Kulmala, M., Kurten, A., Lehtipalo, K., Makhmutov, V., Molteni, U., Rissanen, M. P., Stozkhov, Y., Trostl, J., Tsagkogeorgas, G., Wagner, R., Williamson, C., Wimmer, D., Winkler, P. M., Yan, C., and Carslaw, K. S.: Causes and importance of new particle formation in the present-day and preindustrial atmospheres, J. Geophys. Res.-Atmos., 122, 8739–8760, https://doi.org/10.1002/2017JD026844, 2017.

Hong, J., Tang, M., Wang, Q., Ma, N., Zhu, S., Zhang, S., Pan, X., Xie, L., Li, G., Kuhn, U., Yan, C., Tao, J., Kuang, Y., He, Y., Xu, W., Cai, R., Zhou, Y., Wang, Z., Zhou, G., Yuan, B., Cheng, Y., and Su, H.: Measurement report: Wintertime new particle formation in the rural area of the North China Plain - influencing factors and possible formation mechanism, Atmos. Chem. Phys., 23, 5699–5713, https://doi.org/10.5194/acp-23-5699-2023, 2023.

Hu, X., Yang, G., Liu, Y., Lu, Y., Wang, Y., Chen, H., Chen, J., and Wang, L.: Atmospheric gaseous organic acids in winter in a rural site of the North China Plain, J. Environ. Sci., 113, 190–203, https://doi.org/10.1016/j.jes.2021.05.035, 2022.

Kerminen, V.-M., Chen, X., Vakkari, V., Petaja, T., Kulmala, M., and Bianchi, F.: Atmospheric new particle formation and growth: review of field observations, Environ. Res. Lett., 13, 103003, https://doi.org/10.1088/1748-9326/aadf3c, 2018.

Kirkby, J., Amorim, A., Baltensperger, U., Carslaw, K. S., Christoudias, T., Curtius, J., Donahue, N. M., Haddad, I. E., Flagan, R. C., Gordon, H., Hansel, A., Harder, H., Junninen, H., Kulmala, M., Kürten, A., Laaksonen, A., Lehtipalo, K., Lelieveld, J., Möhler, O., Riipinen, I., Stratmann, F., Tomé, A., Virtanen, A., Volkamer, R., Winkler, P. M., and Worsnop, D. R.: Atmospheric new particle formation from the CERN CLOUD experiment, Nat. Geosci., 16, 948–957, https://doi.org/10.1038/s41561-023-01305-0, 2023.

Kulmala, M., Kokkonen, T., Pekkanen, J., Paatero, S., Petaja, T., Kerminen, V.-M., and Ding, A.: Opinion: Gigacity - a source of problems or the new way to sustainable development, Atmos. Chem. Phys., 21, 8313–8322, https://doi.org/10.5194/acp-21-8313-2021, 2021.

Kürten, A., Li, C., Bianchi, F., Curtius, J., Dias, A., Donahue, N. M., Duplissy, J., Flagan, R. C., Hakala, J., Jokinen, T., Kirkby, J., Kulmala, M., Laaksonen, A., Lehtipalo, K., Makhmutov, V., Onnela, A., Rissanen, M. P., Simon, M., Sipilä, M., Stozhkov, Y., Tröstl, J., Ye, P., and McMurry, P. H.: New particle formation in the sulfuric acid–dimethylamine–water system: reevaluation of CLOUD chamber measurements and comparison to an aerosol nucleation and growth model, Atmos. Chem. Phys., 18, 845–863, https://doi.org/10.5194/acp-18-845-2018, 2018.

Larriba, C., Hogan Jr., C. J., Attoui, M., Borrajo, R., Garcia, J. F., and de la Mora, J. F.: The mobility–volume relationship below 3.0 nm examined by tandem mobility–mass measurement, Aerosol Sci. Tech., 45, 453–467, https://doi.org/10.1080/02786826.2010.546820, 2011.

Li, C., Li, Y., Li, X., Cai, R., Fan, Y., Qiao, X., Yin, R., Yan, C., Guo, Y., Liu, Y., Zheng, J., Kerminen, V.-M., Kulmala, M., Xiao, H., and Jiang, J.: Comprehensive simulations of new particle formation events in Beijing with a cluster dynamics-multicomponent sectional model, Atmos. Chem. Phys., 23, 6879–6896, https://doi.org/10.5194/acp-23-6879-2023, 2023.

Liu, C., Lyu, W., Zhao, W., Zheng, F., and Lu, J.: Exploratory research on influential factors of China's sulfur dioxide emission based on symbolic regression, Environ. Monit. Assess., 195, 41, https://doi.org/10.1007/s10661-022-10595-7, 2023.

Lu, Y., Yan, C., Fu, Y., Chen, Y., Liu, Y., Yang, G., Wang, Y., Bianchi, F., Chu, B., Zhou, Y., Yin, R., Baalbaki, R., Garmash, O., Deng, C., Wang, W., Liu, Y., Petaja, T., Kerminen, V.-M., Jiang, J., Kulmala, M., and Wang, L.: A proxy for atmospheric daytime gaseous sulfuric acid concentration in urban Beijing, Atmos. Chem. Phys., 19, 1971–1983, https://doi.org/10.5194/acp-19-1971-2019, 2019.

Lu, Y., Liu, L., Ning, A., Yang, G., Liu, Y., Kurten, T., Vehkamaki, H., Zhang, X., and Wang, L.: Atmospheric sulfuric acid-dimethylamine nucleation enhanced by trifluoroacetic acid, Geophys. Res. Lett., 47, e2019GL085627, https://doi.org/10.1029/2019GL085627, 2020.

Mohr, C., Thornton, J. A., Heitto, A., Lopez-Hilfiker, F. D., Lutz, A., Riipinen, I., Hong, J., Donahue, N. M., Hallquist, M., Petäjä, T., Kulmala, M., and Yli-Juuti, T.: Molecular identification of organic vapors driving atmospheric nanoparticle growth, Nat. Commun., 10, 4442, https://doi.org/10.1038/s41467-019-12473-2, 2019.

Myllys, N., Kubečka, J., Besel, V., Alfaouri, D., Olenius, T., Smith, J. N., and Passananti, M.: Role of base strength, cluster structure and charge in sulfuric-acid-driven particle formation, Atmos. Chem. Phys., 19, 9753–9768, https://doi.org/10.5194/acp-19-9753-2019, 2019.

https://doi.org/10.5194/egusphere-2025-2787
Preprint. Discussion started: 4 July 2025

Olenius, T., Halonen, R., Kurten, T., Henschel, H., Kupiainen-Maata, O., Ortega, I. K., Jen, C. N., Vehkamaki, H., and Riipinen, I.: New particle formation from sulfuric acid and amines: Comparison of monomethylamine, dimethylamine, and trimethylamine, J. Geophys. Res.-Atmos., 122, 7103–7118, https://doi.org/10.1002/2017JD026501, 2017.

Ortega, I. K., Kupiainen, O., Kurtén, T., Olenius, T., Wilkman, O., McGrath, M. J., Loukonen, V., and Vehkamäki, H.: From quantum chemical formation free energies to evaporation rates, Atmos. Chem. Phys., 12, 225–235, https://doi.org/10.5194/acp-12-225-2012, 2012.

Qiao, X., Yan, C., Li, X., Guo, Y., Yin, R., Deng, C., Li, C., Nie, W., Wang, M., Cai, R., Huang, D., Wang, Z., Yao, L., Worsnop, D. R., Bianchi, F., Liu, Y., Donahue, N. M., Kulmala, M., and Jiang, J.: Contribution of atmospheric oxygenated organic compounds to particle growth in an urban environment, Environ. Sci. Technol., 55, 13646–13656, https://doi.org/10.1021/acs.est.1c02095, 2021.

Ren, S., Yao, L., Wang, Y., Yang, G., Liu, Y., Li, Y., Lu, Y., Wang, L., and Wang, L.: Volatility parameterization of ambient organic aerosols a a rural site of the North China Plain, Atmos. Chem. Phys., 22, 9283–9297, https://doi.org/10.5194/acp-22-9283-2022, 2022.

Shang, D., Hu, M., Wang, X., Tang, L., Clusius, P. S., Qiu, Y., Yu, X., Chen, Z., Zhang, Z., Sun, J., Dao, X., Zeng, L., Guo, S., Wu, Z., and Boy, M.: Spatial inhomogeneity of new particle formation in the urban and mountainous atmospheres of the North China Plain during the 2022 Winter Olympics, Atmosphere, 14, 1395, https://doi.org/10.3390/atmos14091395, 2023.

Simon, M., Dada, L., Heinritzi, M., Scholz, W., Stolzenburg, D., Fischer, L., Wagner, A. C., Kuerten, A., Rorup, B., He, X.-C., Almeida, J., Baalbaki, R., Baccarini, A., Bauer, P. S., Beck, L., Bergen, A., Bianchi, F., Brakling, S., Brilke, S., Caudillo, L., Chen, D., Chu, B., Dias, A., Draper, D. C., Duplissy, J., El-Haddad, I., Finkenzeller, H., Frege, C., Gonzalez-Carracedo, L., Gordon, H., Granzin, M., Hakala, J., Hofbauer, V., Hoyle, C. R., Kim, C., Kong, W., Lamkaddam, H., Lee, C. P., Lehtipalo, K., Leiminger, M., Mai, H., Manninen, H. E., Marie, G., Marten, R., Mentler, B., Molteni, U., Nichman, L., Nie, W., Ojdanic, A., Onnela, A., Partoll, E., Petaja, T., Pfeifer, J., Philippov, M., Quelever, L. L. J., Ranjithkumar, A., Rissanen, M. P., Schallhart, S., Schobesberger, S., Schuchmann, S., Shen, J., Sipila, M., Steiner, G., Stozhkov, Y., Tauber, C., Tham, Y. J., Tome, A. R., Vazquez-Pufleau, M., Vogel, A. L., Wagner, R., Wang, M., Wang, D. S., Wang, Y., Weber, S. K., Wu, Y., Xiao, M., Yan, C., Ye, P., Ye, Q., Zauner-Wieczorek, M., Zhou, X., Baltensperger, U., Dommen, J., Flagan, R. C., Hansel, A., Kulmala, M., Volkamer, R., Winkler, P. M., Worsnop, D. R., Donahue, N. M., Kirkby, J., and Curtius, J.: Molecular understanding of new-particle formation from α-pinene between -50 and +25°C, Atmos. Chem. Phys., 20, 9183–9207, https://doi.org/10.5194/acp-20-9183-2020, 2020.

Stolzenburg, D., Fischer, L., Vogel, A. L., Heinritzi, M., Schervish, M., Simon, M., Wagner, A. C., Dada, L., Ahonen, L. R., Amorim, A., Baccarini, A., Bauer, P. S., Baumgartner, B., Bergen, A., Bianchi, F., Breitenlechner, M., Brilke, S., Mazon, S. B., Chen, D., Dias, A., Draper, D. C., Duplissy, J., El Haddad, I., Finkenzeller, H., Frege, C., Fuchs, C., Garmash, O., Gordon, H., He, X., Helm, J., Hofbauer, V., Hoyle, C. R., Kim, C., Kirkby, J., Kontkanen, J., Kuerten, A., Lampilahti, J., Lawler, M., Lehtipalo, K., Leiminger, M., Mai, H., Mathot, S., Mentler, B., Molteni, U., Nie, W., Nieminen, T., Nowak, J. B., Ojdanic, A., Onnela, A., Passananti, M., Petaja, T., Quelever, L. L. J., Rissanen, M. P., Sarnela, N., Schallhart, S., Tauber, C., Tome, A., Wagner, R., Wang, M., Weitz, L., Wimmer, D., Xiao, M., Yan, C., Ye, P., Zha, Q., Baltensperger, U., Curtius, J., Dommen, J., Flagan, R. C., Kulmala, M., Smith, J. N., Worsnop, D. R., Hansel, A., Donahue, N. M., and Winkler, P. M.: Rapid growth of organic aerosol nanoparticles over a wide tropospheric temperature range, Proc. Natl. Acad. Sci. U. S. A., 115, 9122–9127, https://doi.org/10.1073/pnas.1807604115, 2018.

Troestl, J., Chuang, W. K., Gordon, H., Heinritzi, M., Yan, C., Molteni, U., Ahlm, L., Frege, C., Bianchi, F., Wagner, R., Simon, M., Lehtipalo, K., Williamson, C., Craven, J. S., Duplissy, J., Adamov, A., Almeida, J., Bernhammer, A.-K., Breitenlechner, M., Brilke, S., Dias, A., Ehrhart, S., Flagan, R. C., Franchin, A., Fuchs, C., Guida, R., Gysel, M., Hansel, A., Hoyle, C. R., Jokinen, T., Junninen, H., Kangasluoma, J., Keskinen, H., Kim, J., Krapf, M., Kuerten, A., Laaksonen, A., Lawler, M., Leiminger, M., Mathot, S., Moehler, O., Nieminen, T., Onnela, A., Petaejae, T., Piel, F. M., Miettinen, P., Rissanen, M. P., Rondo, L., Sarnela, N., Schobesberger, S., Sengupta, K., Sipila, M., Smith, J. N., Steiner, G., Tome, A., Virtanen, A., Wagner, A. C., Weingartner, E., Wimmer, D., Winkler, P. M., Ye, P., Carslaw, K. S., Curtius, J., Dommen, J., Kirkby, J., Kulmala, M., Riipinen, I., Worsnop, D. R., Donahue, N. M., and Baltensperger, U.: The role of low-volatility organic compounds in initial particle growth in the atmosphere, Nature, 533, 527–531, https://doi.org/10.1038/nature18271, 2016.

https://doi.org/10.5194/egusphere-2025-2787
Preprint. Discussion started: 4 July 2025

Wang, Y., Yang, G., Lu, Y., Liu, Y., Chen, J., and Wang, L.: Detection of gaseous dimethylamine using vocus proton-transfer-reaction time-of-flight mass spectrometry, Atmos. Environ., 243, 117875, https://doi.org/10.1016/j.atmosenv.2020.117875, 2020.

Wu, Y., Huo, J., Yang, G., Wang, Y., Wang, L., Wu, S., Yao, L., Fu, Q., and Wang, L.: Measurement report: Production and loss of atmospheric formaldehyde at a suburban site of Shanghai in summertime, Atmos. Chem. Phys., 23, 2997–3014, https://doi.org/10.5194/acp-23-2997-2023, 2023.

Xiao, M., Hoyle, C. R., Dada, L., Stolzenburg, D., Kuerten, A., Wang, M., Lamkaddam, H., Garmash, O., Mentler, B., Molteni, U., Baccarini, A., Simon, M., He, X.-C., Lehtipalo, K., Ahonen, L. R., Baalbaki, R., Bauer, P. S., Beck, L., Bell, D., Bianchi, F., Brilke, S., Chen, D., Chiu, R., Dias, A., Duplissy, J., Finkenzeller, H., Gordon, H., Hofbauer, V., Kim, C., Koenig, T. K., Lampilahti, J., Lee, C. P., Li, Z., Mai, H., Makhmutov, V., Manninen, H. E., Marten, R., Mathot, S., Mauldin, R. L., Nie, W., Onnela, A., Partoll, E., Petaja, T., Pfeifer, J., Pospisilova, V., Quelever, L. L. J., Rissanen, M., Schobesberger, S., Schuchmann, S., Stozhkov, Y., Tauber, C., Tham, Y. J., Tome, A., Vazquez-Pufleau, M., Wagner, A. C., Wagner, R., Wang, Y., Weitz, L., Wimmer, D., Wu, Y., Yan, C., Ye, P., Ye, Q., Zha, Q., Zhou, X., Amorim, A., Carslaw, K., Curtius, J., Hansel, A., Volkamer, R., Winkler, P. M., Flagan, R. C., Kulmala, M., Worsnop, D. R., Kirkby, J., Donahue, N. M., Baltensperger, U., El Haddad, I., and Dommen, J.: The driving factors of new particle formation and growth in the polluted boundary layer, Atmos. Chem. Phys., 21, 14275–14291, https://doi.org/10.5194/acp-21-14275-2021, 2021.

Xiao, S., Wang, M. Y., Yao, L., Kulmala, M., Zhou, B., Yang, X., Chen, J. M., Wang, D. F., Fu, Q. Y., Worsnop, D. R., and Wang, L.: Strong atmospheric new particle formation in winter in urban Shanghai, China, Atmos. Chem. Phys., 15, 1769–1781, https://doi.org/10.5194/acp-15-1769-2015, 2015.

Yang, X., Ren, S., Wang, Y., Yang, G., Li, Y., Li, C., Wang, L., Yao, L., and Wang, L.: Volatility Parametrization of Low-Volatile Components of ambient organic aerosols based on molecular formulas, Environ. Sci. Technol., 57, 11595–11604, https://doi.org/10.1021/acs.est.3c02073, 2023.

Yao, L., Wang, M.-Y., Wang, X.-K., Liu, Y.-J., Chen, H.-F., Zheng, J., Nie, W., Ding, A.-J., Geng, F.-H., Wang, D.-F., Chen, J.-M., Worsnop, D. R., and Wang, L.: Detection of atmospheric gaseous amines and amides by a high-resolution time-of-flight chemical ionization mass spectrometer with protonated ethanol reagent ions, Atmos. Chem. Phys., 16, 14527–14543, https://doi.org/10.5194/acp-16-14527-2016, 2016.

Yao, L., Garmash, O., Bianchi, F., Zheng, J., Yan, C., Kontkanen, J., Junninen, H., Mazon, S. B., Ehn, M., Paasonen, P., Sipila, M., Wang, M., Wang, X., Xiao, S., Chen, H., Lu, Y., Zhang, B., Wang, D., Fu, Q., Geng, F., Li, L., Wang, H., Qiao, L., Yang, X., Chen, J., Kerminen, V.-M., Petaja, T., Worsnop, D. R., Kulmala, M., and Wang, L.: Atmospheric new particle formation from sulfuric acid and amines in a Chinese megacity, Science, 361, 278–281, https://doi.org/10.1126/science.aao4839, 2018.

Yin, R., Yan, C., Cai, R., Li, X., Shen, J., Lu, Y., Schobesberger, S., Fu, Y., Deng, C., Wang, L., Liu, Y., Zheng, J., Xie, H., Bianchi, F., Worsnop, D. R., Kulmala, M., and Jiang, J.: Acid-base clusters during atmospheric new particle formation in urban Beijing, Environ. Sci. Technol., 55, 10994–11005, https://doi.org/10.1021/acs.est.1c02701, 2021.

Yu, H., Zhou, L., Dai, L., Shen, W., Dai, W., Zheng, J., Ma, Y., and Chen, M.: Nucleation and growth of sub-3 nm particles in the polluted urban atmosphere of a megacity in China, Atmos. Chem. Phys., 16, 2641–2657, https://doi.org/10.5194/acp-16-2641-2016, 2016.

Zapadinsky, E., Passananti, M., Myllys, N., Kurtén, T., and Vehkamäki, H.: Modeling on fragmentation of clusters inside a mass spectrometer, J. Phys. Chem. A, 123, 611–624, https://doi.org/10.1021/acs.jpca.8b10744, 2019.

Zhao, B., Donahue, N. M., Zhang, K., Mao, L., Shrivastava, M., Ma, P.-L., Shen, J., Wang, S., Sun, J., Gordon, H., Tang, S., Fast, J., Wang, M., Gao, Y., Yan, C., Singh, B., Li, Z., Huang, L., Lou, S., Lin, G., Wang, H., Jiang, J., Ding, A., Nie, W., Qi, X., Chi, X., and Wang, L.: Global variability in atmospheric new particle formation mechanisms, Nature, 631, 98–105, https://doi.org/10.1038/s41586-024-07547-1, 2024.

Zhou, Y., Hakala, S., Yan, C., Gao, Y., Yao, X., Chu, B., Chan, T., Kangasluoma, J., Gani, S., Kontkanen, J., Paasonen, P., Liu, Y., Petaja, T., Kulmala, M., and Dada, L.: Measurement report: New particle formation characteristics at an urban and a mountain station in northern China, Atmos. Chem. Phys., 21, 17885–17906, https://doi.org/10.5194/acp-21-17885-2021, 2021.